# **Nanoscale**



**PAPER** 

View Article Online
View Journal | View Issue



Cite this: Nanoscale, 2020, 12, 18363

# Beyond conventional nonlinear fracture mechanics in graphene nanoribbons†

Takahiro Shimada, (1) \*a Kai Huang, (1) \*a,b Le Van Lich, (1) a,c Naoki Ozaki, Bongkyun Jang (1) and Takayuki Kitamura

Owing to a finite and single-atom-thick two-dimensional structure, graphene nanostructures such as nanoribbons possess outstanding physical properties and unique size-dependent characteristics due to nanoscale defects, especially for mechanical properties. Graphene nanostructures characteristically exhibit strong nonlinearity in deformation and the defect brings about an extremely localized singular stress field of only a few nanometers, which might lead to unique fracture properties. Fundamental understanding of their fracture properties and criteria is, however, seriously underdeveloped and limited to the level of continuum mechanics and linear elasticity. Here, we demonstrate the breakdown of continuum-based fracture criteria for graphene nanoribbons due to the strong nonlinearity and discreteness of atoms emerging with decreasing size and identify the critical sizes for these conventional criteria. We further propose an energy-based criterion considering atomic discrete nature, and show that it can successfully describe the fracture beyond the critical sizes. The complete clarification of fracture criterion for nonlinear graphene with nanoscale singularity contributes not only to the reliable design of graphene-based nanodevices but also to the elucidation of the extreme dimensional limit in fracture mechanics.

Received 18th May 2020, Accepted 4th August 2020 DOI: 10.1039/d0nr03836a

rsc.li/nanoscale

### Introduction

Since the discovery of graphene, <sup>1</sup> a one-atom-thick layer of sp<sup>2</sup> hybridized carbon atoms, it has been attracting considerable attention and scientific/technological interest as a representative of two-dimensional (2D) materials owing to its exceptional electrical, <sup>1,2</sup> thermal, <sup>3</sup> optical, <sup>4</sup> and mechanical <sup>5,6</sup> properties and its promising applications such as flexible electronic <sup>7,8</sup> or biological devices, nano-electromechanical systems, <sup>10</sup> graphene-reinforced nanocomposites, <sup>11–13</sup> and nitrogen-doped graphene in energy fields. <sup>14</sup> In particular, graphene nanostructures such as graphene nanoribbons (GNRs), <sup>15</sup> tailored from the ideal graphene sheet within a finite dimension, exhibit unique electronic band structures arising from the interplay of the edge and nano-size effects, <sup>16</sup> which enable tuning of the electronic and transport properties of graphene-based nanodevices. <sup>17</sup> Because of fragility due to their

Numerous experimental and theoretical studies have already been carried out to understand the fracture toughness and other properties of large (or infinite) graphene, and they demonstrated that Griffith (or conventional fracture mechanics) theory on the basis of linear elasticity can describe fracture of graphene to some extent in spite of its one-atom-thick layer structure. 18-23 In contrast, the fracture properties of and the fracture criterion for graphene nanostructures are, however, seriously underdeveloped due to atomic-level nonlinearity and continuum-media assumption at the nanoscale. Generally, linear elasticity seems to dominate the fracture of a crack in graphene as nonlinear deformation mainly stems from the atomic bonds in the vicinity of the crack tip. However, such atomic-level nonlinearity plays a crucial role in the fracture of GNRs, and should be fully considered especially as the size extremely shrinks down at the nanoscale. A fundamental question is about the critical size in the transition between linear and nonlinear mechanics at fracture.

Conventional fracture mechanics, established on the basis of continuum assumption, provides criteria to describe the critical conditions under which a crack becomes mechanically unstable and starts to propagate.<sup>24–26</sup> At the nanoscale,

thin structure, characterization and understanding of the fracture properties of graphene nanostructures are, therefore, of central importance for both the reliability of these applications and scientific interest in the deformation physics of panestructures.

<sup>&</sup>lt;sup>a</sup>Department of Mechanical Engineering and Science, Kyoto University, Kyoto 615-8540. Japan. E-mail: shimada@me.kyoto-u.ac.ip

<sup>&</sup>lt;sup>b</sup>Department of Astronautic Science and Mechanics, Harbin Institute of Technology, Harbin 150001, China. E-mail: huangkai@hit.edu.cn

<sup>&</sup>lt;sup>c</sup>School of Materials Science and Engineering, Hanoi University of Science and Technology, Hanoi, Viet Nam

<sup>&</sup>lt;sup>d</sup>Department of Applied Nano-mechanics, Korea Institute of Machinery & Materials, Daeieon 34103 Korea

<sup>†</sup>Electronic supplementary information (ESI) available. See DOI: 10.1039/d0nr03836a

**Paper** Nanoscale

however, the size of the singular stress field, which intrinsically dominates the fracture of a crack, shrinks down to a few nanometers or less, where only an extremely smaller number of atoms exist than that in the macroscale materials. This situation immediately contradicts with the above-mentioned concept of conventional fracture mechanics that postulates the existence of a large enough number of atoms near the crack tip to regard the area as continuum media. This suggests a lower size limit for conventional fracture criteria. Recently, there have been some investigations on the breakdown of fracture criteria for brittle fracture at the nanoscale under simple linear elasticity, 18,19,27-31 whereas GNRs show strong nonlinearity in their deformation. Consideration of nonlinearity is essential to understand the intrinsic breakdown of continuum-based fracture criteria, and in addition a universal criterion beyond the size limit is still critically missing.

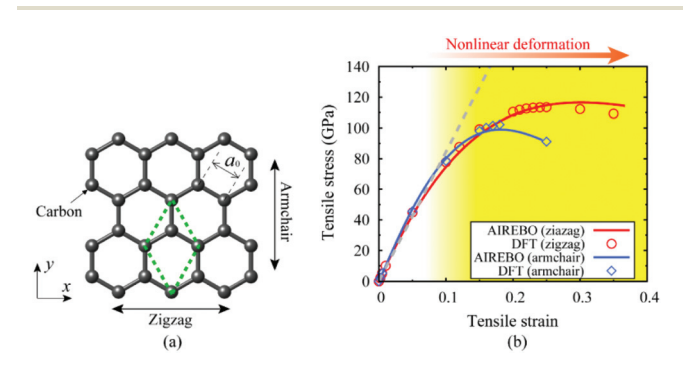


Fig. 1 (a) Atomic configuration of pristine graphene and (b) stressstrain curves of pristine graphene with tensile load along the armchair and zigzag directions.

Here, we demonstrate the breakdown of continuum-based criteria in GNRs by experiments in silico, which originates from the strong nonlinearity and discreteness of atoms emerging dominant with decreasing size. In addition, the critical sizes are identified for these conventional criteria. Furthermore, we propose a new energy-based criterion within the framework of Atomic Fracture Mechanics (AFM) considering discrete atomic nature, and it can successfully describe the fracture beyond the critical sizes in a nonlinear elastic material

## Results and discussion

Graphene shows nonlinear elastic behavior in the stress-strain relationship under large deformation. Under the uniaxial tensions along the zigzag and armchair directions of pristine graphene, shown in Fig. 1a, stress-strain curves are obtained from ab initio calculations based on density functional theory (DFT) and molecular static (MS) simulations. The results in Fig. 1b demonstrate that pristine graphene possesses eminent nonlinear elasticity at the tensile strain larger than 0.1, in both zigzag and armchair directions. Careful evaluation of the stress-strain curve in the zigzag direction clarifies that nonlinearity begins at a stress of  $\sigma_0$  = 48.7 GPa (strain of 0.06). In fracture mechanics of graphene with nanoscale dimensions, the nonlinearity in large deformation is a critical issue because of the existence of few atoms near cracks and defects.

The fracture test of graphene is performed by MS simulation for single-crystalline GNRs with a pre-crack, which shows strong nonlinearity. Fig. 2a shows an atomic model of the specimen with a single edge crack. W, H = 2W and a = W

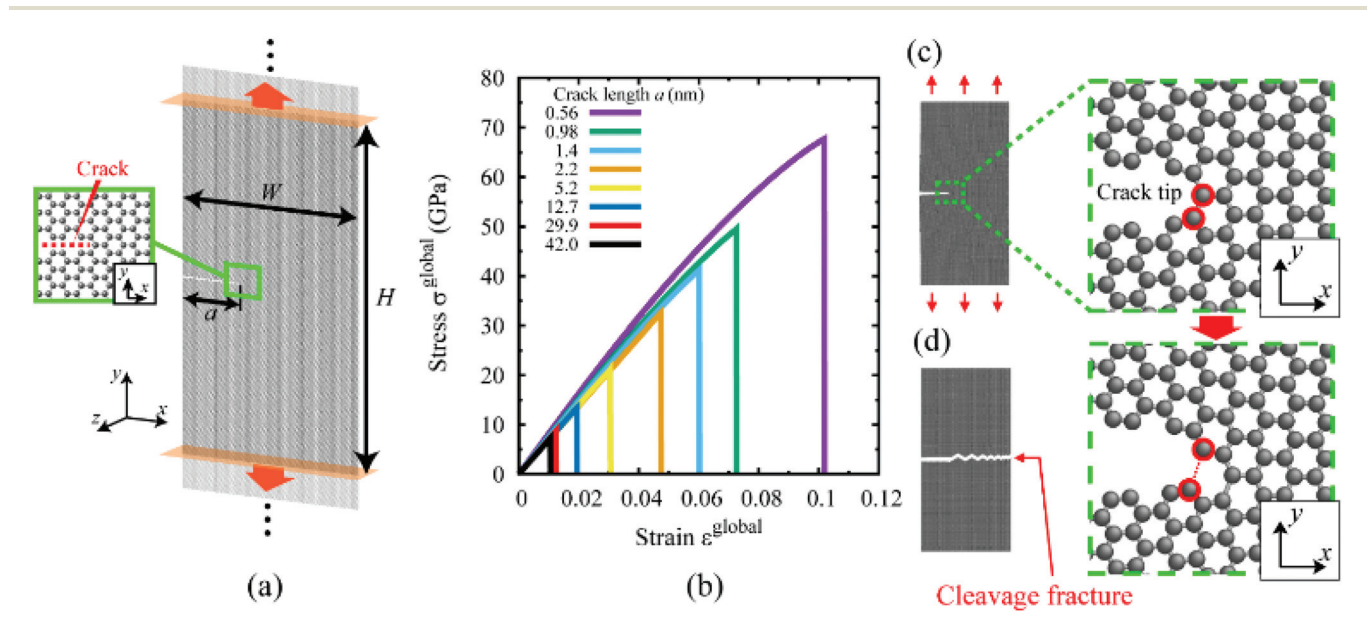


Fig. 2 (a) Geometry and loading conditions of a pre-cracked GNR specimen for tensile test. The crack faces are along the armchair direction. (b) Tensile stress-strain curves of GNR specimens with a crack length of a = 0.56-42.0 nm. (c) and (d) GNR specimen at the onset of crack propagation and after crack propagation, respectively. The insets in (c) show the atomic structures before and immediately after the first carbon bond breaks at the onset of crack propagation. The crack propagates along the armchair direction.

Nanoscale Paper

3) represent the width, the length and the crack length of the specimen, respectively. The crack with armchair edges is modeled by removing an array of atoms from the specimen as shown in the inset of Fig. 2a. Fig. 2b shows the stress-strain curves for graphene specimens with different initial crack lengths (with crack faces all along the armchair direction) under uniaxial tensile tests. During these tests, the global stress increases monotonically with the global strain. Subsequently, the global stress suddenly drops to zero when the global strain reaches a critical value, at which the crack becomes mechanically unstable and begins to propagate. Fig. 2c shows the first sign of failure, in which the first bond to break is at the crack tip. Once this bond has been broken, a complete failure of the specimen proceeds rapidly along the armchair direction, resulting in two fractured pieces (as shown in Fig. 2d), and thus the fracture occurs at mode-I and is purely brittle. Such brittle nature of fracture is observed in all GNR specimens under tension, regardless of the crack length. However, as the crack length increases, both the critical global stress and strain decrease. The characteristics of the brittle fracture obtained here are consistent with those of simulated predictions<sup>18,19</sup> and recent experimental observations, <sup>19,20</sup> which confirms the reliability of the present tests.

In investigations of crack propagation in GNRs, it has been widely believed that nonlinear deformation is highly localized near the crack tip since graphene begins to rupture at a small global strain where the linear behavior seemingly dominates, and therefore linear elasticity is often adopted to analyze crack problems in graphene for the sake of simplicity. The tensile results in the present study are thus firstly analyzed based on linear elastic fracture mechanics (LEFM) approach by considering the material as a linear elastic continuum. In the GNR specimen with a crack length of a = 42.0 nm, the stress intensively concentrates near the crack tip and forms a singular field inversely proportional to the square root of the distance r, i.e.,  $\sigma_{yy} = K_{\rm I}/\sqrt{2\pi r}$ . Here,  $K_{\rm I}$  denotes the stress intensity factor that characterizes the local stress field near the crack tip (Fig. 3a). In addition to the stress intensity approach, an alternative fracture parameter that is based on the energy approach, i.e., the energy release rate (ERR) G, has been frequently used in the LEFM approach as a global fracture characterizing parameter. The ERR is defined as the released mechanical (strain) energy with an infinitesimal increment of the crack cross-section  $\Delta A$ , and LEFM gives

$$G = -\frac{\mathrm{d}\Pi_{\mathrm{LE}}(A)}{\mathrm{d}A} = -\lim_{\Delta A \to 0} \frac{\Pi_{\mathrm{LE}}(A + \Delta A) - \Pi_{\mathrm{LE}}(A)}{\Delta A} \tag{1}$$

where  $\Pi_{LE}(A)$  denotes the strain energy under the assumption of linear-elastic continuum media and A the crack crosssection. For linear elastic materials fractured under mode-I, G uniquely correlates with the stress intensity factor  $K_{\rm I}$  as G = $K_1^2/E$ , where E is Young's modulus. Fig. 3b plots the ERR at fracture  $G^{f}$  as a function of crack length for all of the GNRs tested. It should be noted that the critical ERR or fracture toughness of (infinite) graphene is evaluated from preliminary simulations to be  $G_C = 11.8 \text{ J m}^{-2} (K_C = 3.15 \text{ MPa m}^{1/2})$  as indi-

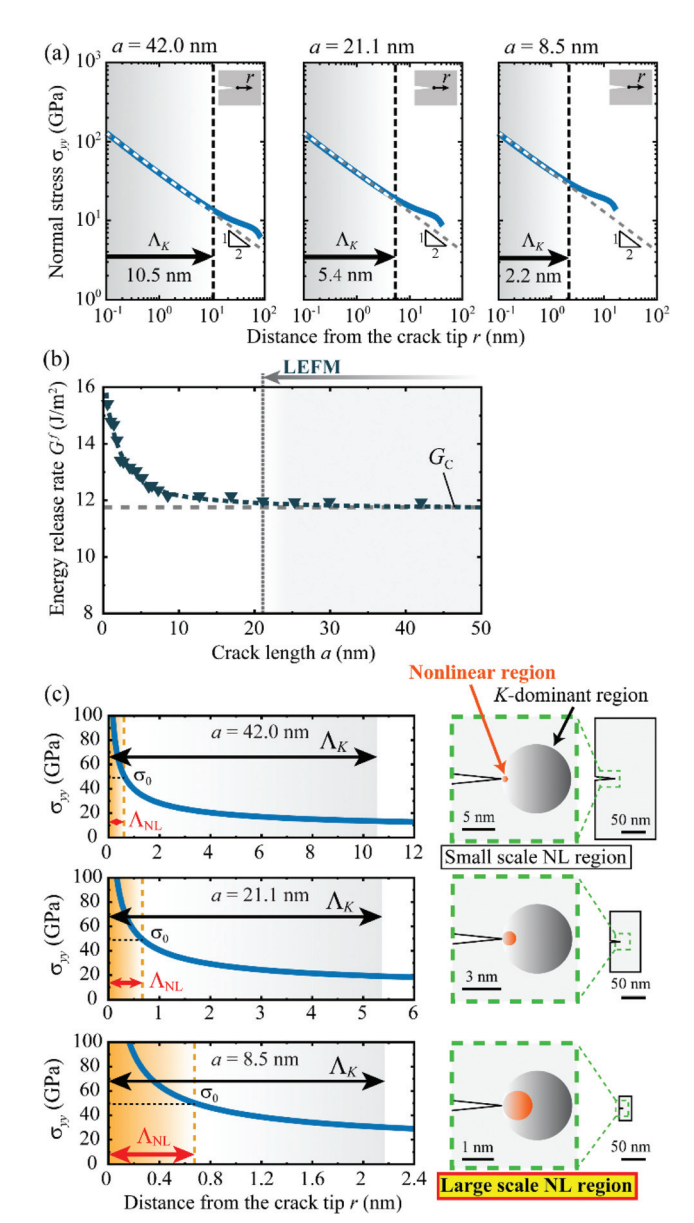


Fig. 3 (a) Normal stress at the onset of fracture as a function of distance from the crack tip r.  $\Lambda_K$  indicates the region of the singular stress field near the crack tip. (b) Critical energy release rate at fracture based on the linear elastic fracture mechanics (LEFM) as a function of crack length a. (c) Comparison between the region of the singular stress field (K-dominant region),  $\Lambda_K$  and the region of nonlinear deformation,  $\Lambda_{NL}$ . Note that the schematic diagrams here mainly illustrate the sizes (but not the exact shapes) of the K-dominant region and the NL region.

cated by the dashed line in Fig. 3b, which is in good agreement with the fracture toughness from previous simulated predictions<sup>21-23</sup> and experimentally measured values.<sup>19</sup> Fig. 3b shows that  $G^{f}$  is consistent with the fracture toughness  $G_{C}$  at large crack lengths (a > 21.1 nm). This consistency evidently indicates that the LEFM criterion, i.e., the crack begins to propagate just when the ERR (or the stress intensity factor) reaches the fracture toughness, is applicable. However, below the crack length as a < 21.1 nm,  $G^f$  begins to deviate from the fracture toughness  $G_{C}$ , which implies that LEFM fails to

Paper Nanoscale

describe the critical condition at which the crack starts to propagate. Therefore, fracture in such GNRs is no longer governed by the ERR, i.e., the breakdown of LEFM. The critical size of LEFM can be evaluated at a crack length of about 20 nm from Fig. 3b.

To shed light on the lower limit of LEFM, we reconsider the long-held yet vague belief that the nonlinear region near the crack tip can be neglected due to its high localization. Fig. 3c shows the region of nonlinear deformation,  $\Lambda_{NL}$ , as compared with the region governed by the singular stress field,  $\Lambda_K$ , for specimens with crack lengths of a = 42.0, 21.1, and 8.5 nm, respectively. The region of nonlinear deformation is determined where the concentrated stress near the crack tip becomes higher than the stress of  $\sigma_0 = 48.7$  GPa. As shown in Fig. 3c, LEFM is valid in the specimen with a large crack length of a = 42.0 nm, where  $\Lambda_K$  is about twenty times larger than  $\Lambda_{NL}$ , and thus large enough to satisfy the hypothesis  $\Lambda_K$  $\gg \Lambda_{\rm NL}$ . On the other hand,  $G^{\rm f}$  starts to deviate for the specimen with a small crack length of a = 21.1 nm, where  $\Lambda_K$ becomes closer to  $\Lambda_{NL}$ , and the hypothesis of LEFM thus breaks down. In fact, the deviation of  $G^{f}$  is more dramatically pronounced around  $\Lambda_K \approx \Lambda_{\rm NL}$ . Therefore,  $\Lambda_K$  determines the lower limit of LEFM, which is roughly estimated to be  $\Lambda_K^{\rm C}$  =  $5\Lambda_{\rm NL} = 5.4$  nm.

Evidently, the nonlinear elastic regime plays an important role in the description of fracture in GNRs, and the nonlinear effect should be taken into account, especially for specimens with a short crack. This, however, shatters the long-held belief of the negligible nonlinear region near the crack tip in GNRs. We thus progress to analyze the tensile results in the present study based on the nonlinear fracture mechanics (NLFM) by considering the material as a nonlinear elastic continuum. According to NLFM, J-integral is considered to be a fracture characterizing parameter for nonlinear materials, which is defined in a similar manner to G in elastic materials, given  $bv^{32}$ 

$$J = -\frac{\mathrm{d}\Pi_{\mathrm{NL}}(A)}{\mathrm{d}A} = -\lim_{\Delta A \to 0} \frac{\Pi_{\mathrm{NL}}(A + \Delta A) - \Pi_{\mathrm{NL}}(A)}{\Delta A}$$
$$= \oint_{\Gamma} \left[ w \mathrm{d}y - T \cdot \frac{\partial u}{\partial x} \mathrm{d}\Gamma \right] \tag{2}$$

where  $\Pi_{NL}(A)$  denotes the nonlinear strain energy of continuum media,  $\Gamma$  arbitrary contour around the tip of a crack, Ttraction vector, and w strain energy density. J-Integral is pathindependent as demonstrated in Fig. S1 (provided in the ESI $\dagger$ ). Fig. 4a plots *J*-integral at fracture  $J^{f}$  as a function of crack length for all of the GNRs tested.  $J^{f}$  is consistent with the fracture toughness  $J_C$  (=  $G_C$ ) and thus the NLFM concept is applicable for GNRs with large crack lengths (a > 21.1 nm). Interestingly, the NLFM concept is still valid for a very short crack of a = 7.3 nm. Below this crack length, however,  $J^{f}$  begins to deviate from the fracture toughness  $J_C$ , which indicates that the NLFM fails to describe the fracture in GNRs. Therefore, fracture in such GNRs is no longer governed by J-integral, i.e., the breakdown of NLFM. The critical size of NLFM can be eval-

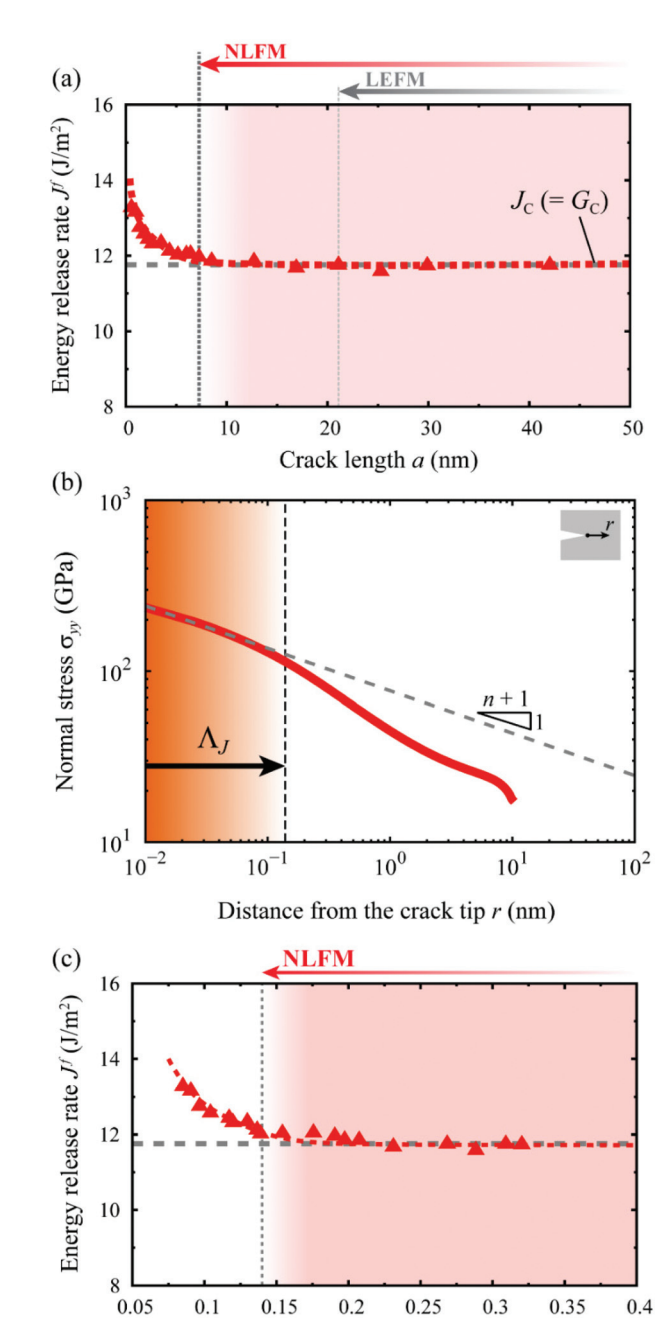


Fig. 4 (a) Critical J-integral at fracture based on nonlinear elastic fracture mechanics (NLFM) as a function of crack length a. (b) Normal stress at the onset of fracture as a function of distance from the crack tip r for a specimen with a = 5.2 nm.  $\Lambda_J$  indicates the region of the HRR singular stress field near the crack tip. (c) Critical J-integral at fracture based on nonlinear elastic fracture mechanics (NLFM) as a function of  $\Lambda_J$ .

*J*-dominant region  $\Lambda_I$  (nm)

uated at a crack length of a = 7.3 nm from Fig. 4a, which is approximately one third of that of LEFM.

To provide physical insight into the lower limit of NLFM, we consider the stress field near the crack tip. Although the stress also intensively concentrates near the crack tip (Fig. 4b) as in LEFM, the stress forms a singular field that is proportional to  $r^{-1/(n+1)}$ , *i.e.*, the HRR (Hutchinson-RiceNanoscale Paper

Rosengren) singular stress field, rather than that of  $r^{-1/2}$  in LEFM. The HRR singular stress field is expressed as 33,34

$$\sigma_{ij}(r) = \left(\frac{J}{r}\right)^{1/(n+1)} \tilde{\sigma}_{ij}(\theta, n) \quad (i, j = x, y)$$
 (3)

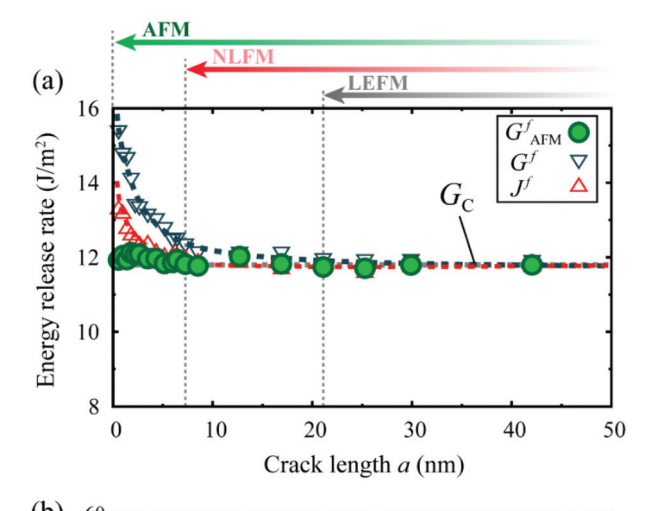
where *n* is the work hardening coefficient and  $\tilde{\sigma}_{ii}(\theta,n)$  the dimensionless function of n and  $\theta$ . Similar to the key dimension of  $\Lambda_K$  in LEFM to determine the lower limit of LEFM, here the area where the stress varies as  $r^{-1/(n+1)}$  is called the *J*-dominated region  $\Lambda_J$ . Fig. 4b shows that the HRR singular stress field still dominates the stress field in the vicinity of the crack tip, even though the crack length is lower than its critical size of 7.3 nm. Thus, the J-integral is sound for the description of the stress field for a short crack even below the critical length. Fig. 4c plots *I*-integral at fracture *I*<sup>f</sup> as a function of J-dominated region  $\Lambda_I$  for all of the specimens. Surprisingly,  $J^t$ is still consistent with the fracture toughness  $J_C$  (=  $G_C$ ), and the NLFM concept is applicable despite the quite small *J*-dominated region, as  $\Lambda_I = 0.14$  nm that is almost equal to the distance between the two carbon atoms in graphene. However, below this size J<sup>f</sup> deviates from the intrinsic fracture toughness. Therefore, the critical size of NLFM can be characterized by  $\Lambda_I^C$ , which is evaluated to be  $\Lambda_I^C = 0.14$  nm.

Because of the breakdown of both LEFM and NLFM (or fracture mechanics in general) in description of fracture in GNRs below the critical sizes, an alternative parameter beyond the continuum-based fracture mechanics that can characterize fracture in GNRs at a scale below the limitation or if possible can even characterize fracture at any scale is urgently required. Here, we propose the following atomic ERR, denoted as  $G_{AEM}$ , as an effective parameter to describe fracture below the lower size limit, which fully takes into account the discreteness of atoms at the crack tip by a straightforward extension of the fracture mechanics concept to the atomic scale, as

$$G_{\text{AFM}} = -\frac{\Delta \Pi_{\text{Atom}}(A)}{\Delta A} = -\frac{\Pi_{\text{Atom}}(A + \Delta A) - \Pi_{\text{Atom}}(A)}{\Delta A}$$
(4)

where  $\Pi_{Atom}(A)$  is the potential energy of the simulated atomic specimen with a crack cross-section of A.  $\Delta A$  is the finite change of the crack cross-section at the onset of fracture, and in the present case, it corresponds to a single bond break at the crack tip as shown in Fig. 2c. In contrast to the original ERR (or J-integral) that is a measure of the continuum strain energy available for an infinitesimal crack extension, the proposed atomic ERR  $G_{AFM}$  accounts for the strain energy of the discretized atomic body and the discrete nature of atoms at the crack-tip, and moreover the effect of shear mode around the crack tip (if any) will also be included. Here we call this analytic theory Atomic Fracture Mechanics (AFM). In addition,  $G_{AFM}$  no longer postulates the presence of a singular field, suggesting its applicability to even non-crack systems.

The atomic ERR at fracture  $G_{AFM}^f$  as a function of crack length a is shown in Fig. 5a, and it clearly indicates that the fracture event always occurs when  $G_{AFM}^{f}$  reaches a critical constant value of 11.8 J m<sup>-2</sup> for all GNRs regardless of their sizes.



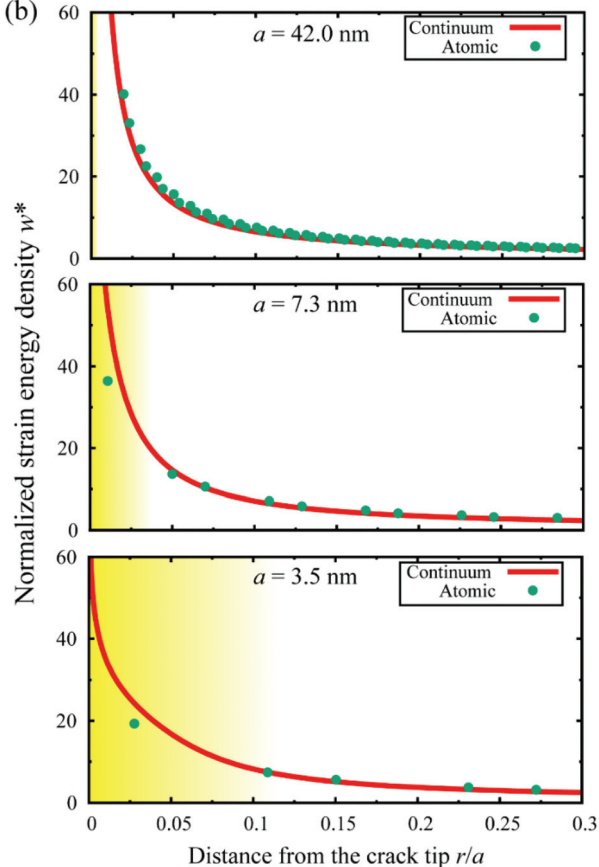


Fig. 5 (a) Critical energy release rate at fracture based on atomic fracture mechanics (AFM), linear elastic fracture mechanics (LEFM), and nonlinear elastic fracture mechanics (NLFM) as a function of crack length a. (b) Comparison of strain energy density distributions near the crack tip between the continuum assumption and the actual atomic specimen under critical loading conditions.

The good consistency between  $G_{AFM}^f$  and continuum-based  $G^f$ (or  $f^{t}$ ) for large crack lengths (a > 21.1 nm) where continuum criteria still work implies that the effect of shear mode on the first bond breaking at the crack tip is negligible. The AFM therefore successfully describes the onset of fracture in GNRs where both the LEFM and NLFM are no longer valid. More

Paper Nanoscale

interestingly,  $G_{AFM}^{f}$  effectively works as a universal fracture characterizing parameter that is not only at the nanoscale but also at the macroscale. As shown in Fig. 5(b), the strain energy distribution by continuum assumption deviates from the actual atomic one at the shortest distance from the crack tip, because continuum theories assume singularity near the crack tip and cannot take into account the crack-tip atomic features, such as surfaces with an opening angle and structural rearrangement. These effects could not be neglected for extremely small specimens, e.g., a = 7.3 nm and a = 3.5 nm. However, as the specimen size approaches the macroscale, the strain energy distribution near the crack-tip is relatively well approximated by continuum assumption  $(\Delta \Pi_{Atom}(A) \approx$  $\Delta\Pi_{\text{Cont}}(A)$ ; a = 42.0 nm), and the finite  $\Delta A$  can be approximately regarded as an infinitesimal value concerning the entire size of the specimen ( $\Delta A \rightarrow 0$ ). Thus,  $G_{AFM}$  is identical to G from LEFM or J-integral from NLFM at the macroscale from eqn (1), (2), and (4). This is apparently rational since the critical  $G_{\rm AFM}^{\rm f}$  of 11.8 J m  $^{-2}$  at fracture is identical to the fracture toughness  $G_C = 11.8 \text{ J m}^{-2}$  obtained by the continuum fracture mechanics. Therefore, the proposed concept of  $G_{AFM}$  consistently and seamlessly bridges the nanoscale (atomic) and the macroscale (continuum), and completely describes fracture in graphene nanostructures for all scales.

## Conclusions

In summary, we have demonstrated the breakdown of the continuum-based fracture theories and showed the lower dimensional limits with regard to fracture in GNRs. The results show that Griffith (or LEFM) and J-integral (or NLFM) criteria fail to describe fracture in GNRs below the critical singular-field sizes of 5.4 nm and 0.14 nm, respectively, which quantitatively elucidates the effect of nonlinearity in deformation on the applicability of continuum-based theory at the nanoscale. To address ultimately these issues, we have proposed a new energy-based theory that accounts for the discrete nature of atoms, and demonstrated that it universally describes fracture even below the critical size for NLFM. The complete clarification of fracture criterion for nonlinear graphene with nanoscale singularity contributes not only to the reliable design of graphenebased nanodevices but also to the elucidation of the extreme dimensional limit in fracture mechanics.

# **Experimental section**

#### Tensile tests for pristine graphene using ab initio calculations

Fig. S2 (provided in the ESI†) expresses a single-layer pristine graphene model for ab initio calculations based on DFT35 using the Vienna ab initio simulation package (VASP).<sup>36</sup> The projector-augmented wave (PAW) potential is employed for electron-ion interaction.<sup>37</sup> The exchange-correlation term is evaluated using the generalized gradient approximation (GGA) of the Perdew-Bruke-Ernzerhof (PBE) formulation. A cubic cell

shown in ESI Fig. S2a† constructs a single-layer graphene tensile specimen by applying a periodic boundary condition for the unit cell in the directions of x and y axes. A zigzag direction and an armchair direction are defined as the x and yaxes in ESI Fig. S2b,† respectively. After applying an infinitesimal strain in the zigzag or armchair direction, the atomic structure is fully relaxed by controlling the cell size until the stress components except in the tensile direction are less than 10 MPa. During the simulation, the cell size in the z direction is maintained as 1 nm.

#### Mode I tensile tests for graphene using MS simulations

For the calculation of the stress-strain relationship of graphene in the zigzag and armchair directions, a periodic hexagonal honeycomb structure with a lattice constant of  $a_0$  = 0.14 nm is constructed as shown in Fig. 1a. The thickness of monolayer graphene is regarded as 0.335 nm, which is the average interlayer distance of graphite. The zigzag direction and armchair direction are defined as x axis and y axis, respectively. The interactions between the carbon atoms are described by the AIREBO (Adaptive Intermolecular Reactive Empirical Bond-Order) potential.<sup>38</sup> The results show good agreement with those of the ab initio calculations (as shown in Fig. 1b), which demonstrates that the AIREBO potential can precisely describe the mechanical behavior of graphene, especially its nonlinear elastic behavior.

For the fracture test of GNRs, a single-edge crack with armchair edges is introduced by removing an array of atoms from the specimen as shown in Fig. 2a. W, H = 2W and a = W/3represent the width, length and crack length of the specimen, respectively. The crack length a varies from 0.56 nm to 42.0 nm. By calculating the stress for each atom, we investigate the fracture characteristics of nanoscale graphene.

Quasi-static tensile tests for single crystalline graphene and pre-cracked GNRs are performed in silico by means of MS simulation using the Large-scale Atomic/Molecular Massively Parallel Simulator (LAMMPS) code. 39 A stepwise increment of infinitesimal strain applied to the specimen is used, and the atomic structure is fully relaxed until the atomic force of interaction between all atoms becomes less than  $1.0 \times 10^{-3}$  eV Å<sup>-1</sup> for each increment. The atomistic simulation will be terminated at the critical deformation  $d_{\rm C}$  when the pre-cracked specimen fractures. The displacement-controlled tensile test realizes mode-I cracking in the pre-cracked GNR specimen.

#### Finite element analysis

The continuum stress distribution at the onset of fracture is obtained by finite element analysis. We perform the linear elastic analysis with the elastic constants of graphene, E = 844GPa and  $\nu = 0.34$ , which are obtained from the MS simulation using the AIREBO potential. Fig. S3 (provided in the ESI†) shows the finite element model of graphene with a single-edge crack. In the model, the bottom part of the specimen is fixed, and the top part is applied to uniform displacement  $d_{\rm C}$ . The dimensions of the specimen are the same as those for the MS simulation as shown in Fig. 2a. In addition, the minimum

mesh size is determined to be less than  $10^{-6}$  of the crack length a to calculate the stress precisely. For a critical displacement  $d_{\rm C}$ , we obtained the stress distributions of the specimen at the failure. Finite element analysis is performed for single-layer graphene using both linear and nonlinear elastic constitutive relationships.

In the nonlinear elastic analysis, it is assumed that the stress-strain relationship obeys Ramberg-Osgood equation<sup>40</sup>

$$E\varepsilon = \sigma + \alpha \left(\frac{\sigma}{\sigma_0}\right)^{n-1} \sigma \tag{5}$$

Here, Young's modulus (E = 844 GPa) and the yield stress ( $\sigma_0 = 48.7$  GPa) are calculated from the AIREBO potential for nonlinear elastic graphene. The nonlinear stress–strain curves in the zigzag direction shown in Fig. 1b are fitted to eqn (5). The fitted parameters are the work hardening coefficient, n = 4.26, and the yield offset,  $\alpha = 3.31 \times 10^{-2}$ .

# Conflicts of interest

There are no conflicts to declare.

# Acknowledgements

The authors acknowledge financial support by the Grant-in-Aid for Specially Promoted Research (Grant number 25000012) and Scientific Research(s) (Grant number 18H05241) from the Japan Society of Promotion of Science (JSPS), and from the China Postdoctoral Science Foundation (Grant number 2019M661267).

## References

- 1 K. S. Novoselov, A. K. Geim, S. V. Morozov, D. Jiang, Y. Zhang, S. V. Dubonos, I. V. Grigorieva and A. A. Firsov, *Science*, 2004, **306**, 666–669.
- 2 Y. Zhang, Y.-W. Tan, H. L. Stomer and P. Kim, *Nature*, 2005, 438, 201–204.
- 3 A. A. Balandin, S. Ghosh, W. Bao, I. Calizo, D. Teweldebrhan, F. Miao and C. N. Lau, *Nano Lett.*, 2008, 8, 902–907.
- 4 R. R. Nair, P. Blake, A. N. Grigorenko, K. S. Novoselov, T. J. Booth, T. Stauber, N. M. R. Peres and A. K. Geim, *Science*, 2008, 320, 1308.
- 5 C. Lee, X. Wei, J. W. Kysar and J. Hone, *Science*, 2008, 321, 385–388.
- 6 E. Cadelano, P. L. Palla, S. Giordano and L. Colombo, *Phys. Rev. Lett.*, 2009, **102**, 235502.
- 7 H. Jang, Y. J. Park, X. Chen, T. Das, M.-S. Kim and J.-H. Ahn, Adv. Mater., 2016, 28, 4184–4202.
- 8 Z. Jin, W. Sun, Y. Ke, C.-J. Shih, G. L. C. Paulus, Q. H. Wang, B. Mu, P. Yin and M. S. Strano, *Nat. Commun.*, 2013, 4, 1663.

- 9 D. Rodrigo, O. Limaj, D. Janner, D. Etezadi, F. J. García de Avajo, V. Pruneri and H. Altug, *Science*, 2015, **349**, 165– 168.
- 10 J. S. Bunch, A. M. van der Zande, S. S. Verbridge, I. W. Frank, D. M. Tanenbaum, J. M. Parpia, H. G. Craighead and P. L. McEuen, *Science*, 2007, 315, 490– 493.
- 11 D. V. Kosynkin, A. L. Higginbotham, A. Sinitskii, J. R. Lomeda, A. Dimiev, B. K. Price and J. M. Tour, *Nature*, 2009, 458, 872–876.
- 12 S.-K. Chien, Y.-T. Yang and C.-K. Chen, *Nanoscale*, 2011, 3, 4307–4313.
- 13 P. Liu, Z. Jin, G. Katsukis, L. W. Drahushuk, S. Shimizu, C.-J. Shih, E. D. Wetzel, J. K. Taggart-Scarff, B. Qing, K. J. Van Vliet, R. Li, B. L. Wardle and M. S. Strano, *Science*, 2016, 353, 364–367.
- 14 H. Xu, L. Ma and Z. Jin, *J. Energy Chem.*, 2018, 27, 146–160.
- 15 J. Cai, P. Ruffieux, R. Jaafar, M. Bieri, T. Braun, S. Blankenburg, M. Muoth, A. P. Seitsonen, M. Saleh, X. Feng, K. Müllen and R. Fasel, *Nature*, 2010, 466, 470– 473.
- 16 Y.-W. Son, M. L. Cohen and S. G. Louie, *Phys. Rev. Lett.*, 2006, 97, 216803.
- 17 M. Y. Han, B. Özylmaz, Y. Zhang and P. Kim, *Phys. Rev. Lett.*, 2007, **98**, 206805.
- 18 H. Yin, H. J. Qi, F. Fan, T. Zhu, B. Wang and Y. Wei, *Nano Lett.*, 2015, 15, 1918–1924.
- 19 P. Zhang, L. Ma, F. Fan, Z. Zeng, C. Peng, P. E. Loya, Z. Liu, Y. Gong, J. Zhang, X. Zhang, P. M. Ajayan, T. Zhu and J. Lou, *Nat. Commun.*, 2014, 5, 3782.
- 20 B. Jang, A. E. Mag-isa, J.-H. Kim, B. Kim, H.-J. Lee, C.-S. Oh, T. Sumigawa and T. Kitamura, *Extreme Mech. Lett.*, 2017, 14, 10–15.
- 21 A. Shekhawat and R. O. Ritchie, *Nat. Commun.*, 2016, 7, 10546.
- 22 A. Tabarraei, X. Wang and D. Jia, *Comput. Mater. Sci.*, 2016, **121**, 151–158.
- 23 D. Datta, S. P. V. Nadimpalli, Y. Li and V. B. Shenoy, *Extreme Mech. Lett.*, 2015, 5, 10–17.
- 24 A. A. Griffith, *Philos. Trans. R. Soc. London, Ser. A*, 1920, 221, 163–198.
- 25 E. Orowan, Rep. Prog. Phys., 1949, 12, 185-232.
- 26 G. R. Irwin and J. A. Kies, Welding J. Res. Suppl., 1954, 33, 193–198.
- 27 T. Shimada, K. Ouchi, Y. Chihara and T. Kitamura, *Sci. Rep.*, 2015, 5, 8596.
- 28 K. Huang, T. Shimada, N. Ozaki, Y. Hagiwara, T. Sumigawa, L. Guo and T. Kitamura, *Int. J. Solids Struct.*, 2017, **128**, 67–72.
- 29 P. Gallo, Adv. Theory Simul., 2019, 2, 1900146.
- 30 P. Gallo, Y. Hagiwara, T. Shimada and T. Kitamura, *Theor. Appl. Fract. Mech.*, 2019, **103**, 102300.
- 31 T. Sumigawa, T. Shimada, S. Tanaka, H. Unno, N. Ozaki, S. Ashida and T. Kitamura, *ACS Nano*, 2017, **11**, 6271–6276.
- 32 J. R. Rice, J. Appl. Mech., 1968, 35, 379-386.

Paper Nanoscale

- 33 J. R. Rice and G. F. Rosengren, *J. Mech. Phys. Solids*, 1968, **16**, 1–12.
- 34 J. W. Hutchinson, J. Mech. Phys. Solids, 1968, 16, 13–31.
- 35 P. Hohenberg and W. Kohn, *Phys. Rev.*, 1964, **136**, B864-B871.
- 36 G. Kresse and J. Hafner, *Phys. Rev. B: Condens. Matter Mater. Phys.*, 1993, 47, 558–561.
- 37 P. E. Blöchl, *Phys. Rev. B: Condens. Matter Mater. Phys.*, 1994, **50**, 17953–17979.
- 38 S. J. Stuart, A. B. Tutein and J. A. Harrison, *J. Chem. Phys.*, 2000, **112**, 6472–6486.
- 39 S. J. Plimpton, J. Comput. Phys., 1995, 117, 1–19.
- 40 W. Ramberg and W. R. Osgood, NACA, Tech. Note, 1943, 902.